

PQM: A Point Quality Evaluation Metric for Dense Maps

Yash Turkar, Pranay Meshram, Charuvahan Adhivarahan, Karthik Dantu

Abstract—LiDAR-based mapping/reconstruction are important for various applications, but evaluating the quality of the dense maps they produce is challenging. The current methods have limitations, including the inability to capture completeness, structural information, and local variations in error. In this paper, we propose a novel point quality evaluation metric (PQM) that consists of four sub-metrics to provide a more comprehensive evaluation of point cloud quality. The completeness sub-metric evaluates the proportion of missing data, the artifact score sub-metric recognises and characterizes artifacts, the accuracy sub-metric measures registration accuracy, and the resolution sub-metric quantifies point cloud density. Through an ablation study using a prototype dataset, we demonstrate the effectiveness of each of the sub-metrics and compare them to popular point cloud distance measures. Using three LiDAR SLAM systems to generate maps, we evaluate their output map quality and demonstrate the metric’s robustness to noise and artifacts. Our implementation of PQM, datasets and detailed documentation on how to integrate with your custom dense mapping pipeline can be found at github.com/droneslab/pqm

I. INTRODUCTION

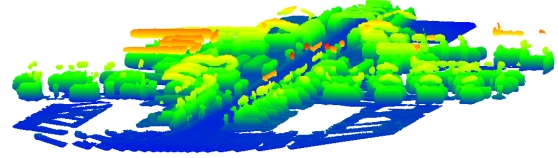
Dense maps play a crucial role in numerous applications including but not limited to autonomous driving, search and rescue, service robotics, and augmented reality. Among the different ways to build dense maps, dense SLAM is particularly interesting due to its ability to produce high-fidelity maps as point clouds that are used for tasks such as localization, re-localization, place recognition, and cross-robot localization but also a need for realtime execution requiring various tradeoffs in map quality. The point clouds produced by these algorithms have been proposed for use in advanced monitoring, sophisticated manipulation, augmented reality, and fine-grained control.

LiDAR-based SLAM methods are increasingly popular thanks to advances in technology. The affordability and improved accuracy of LiDAR sensors now allow for the real-time creation of high-quality, dense point clouds. Fig.2 provides a comparison between point clouds generated using an engineering-grade LiDAR, specifically the Z+F Imager 5016 from the HILTI SLAM dataset [4] (on the left), and an inexpensive Hesai Pandar XT-32 using FAST-LIO2 [1], an online direct registration-based SLAM method (on the right). It is clear from the visual comparison that FAST-LIO2 produces point clouds that are nearly as high-quality as those generated by the engineering-grade LiDAR, which is generally very expensive.

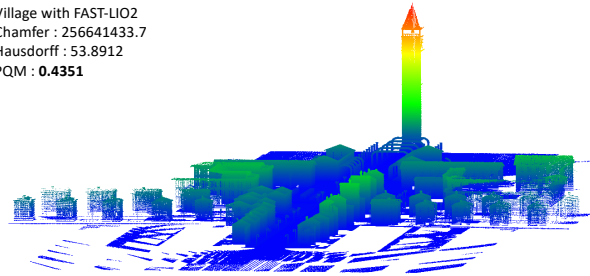
The evaluation of point clouds poses a significant challenge due to the complexity of capturing all aspects of map-

All Authors are with the Department of Computer Science and Engineering, University at Buffalo, Buffalo, NY 14260, USA {yashturk, pranaywa, charuvah, kdantu}@buffalo.edu

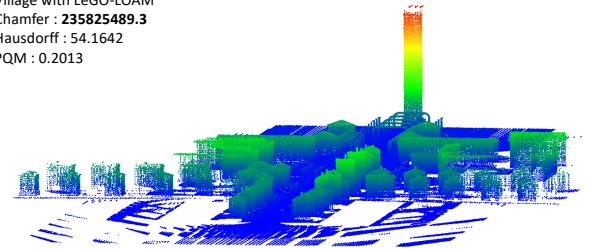
Village with Puma
Chamfer : 2595147655
Hausdorff : **35.0528**
PQM : 0.2089



Village with FAST-LIO2
Chamfer : 256641433.7
Hausdorff : 53.8912
PQM : **0.4351**



Village with LeGO-LOAM
Chamfer : **235825489.3**
Hausdorff : 54.1642
PQM : 0.2013



Village Ground Truth

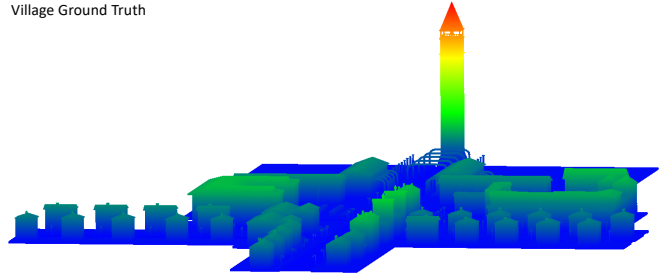


Fig. 1: PQM is the only metric that correctly identifies FAST-LIO2 [1] as having the highest quality among all candidates despite CD and HD indicating LeGO-LOAM [2] and Puma [3] have the highest quality, respectively, in a visual comparison.

ping accuracy. While some measures, such as the Absolute Trajectory Error (ATE), can assess the difference between expected and measured translation and rotation, they do not fully account for map quality and are only indirect measures. Given a reference map, it is important to identify how much of the reference map is captured by a mapping method, how close the created map is to the reference, whether the method created anomalies that do not exist in the reference (we call

these *artifacts*) and if the density of the resultant point cloud is similar to the reference or sparser.

Popular methods for comparing point clouds and meshes such as Chamfer distance (CD), Hausdorff distance (HD), and Earth Mover’s distance (EMD), have limitations. CD is insensitive to point density and significantly influenced by outliers. Therefore, it serves as a poor performance metric to characterize point cloud completeness or map artifacts. On the other hand, while EMD can detect changes in density, the requirement for a one-to-one correspondence between compared maps is usually too strict and can lead to ignoring local fine-grained structural details. Additionally, EMD is significantly more computationally expensive than CD, which can limit its practical applications. Overall, neither CD nor EMD is ideally suitable for evaluating the quality of generated shapes, as they may fail to capture coverage or completeness, structural information, and local variations in error. Therefore, an ideal evaluation method should be efficient and accurately reflect the presence of artifacts or missing data while considering all factors affecting the quality of point clouds for the above applications. A good metric should have the following:

- The metric should capture coverage and completeness of the point cloud, as well as structural information, to provide a comprehensive evaluation of quality.
- The metric should be computationally efficient and handle large datasets to be useful for practical applications
- The metric should accurately penalize artifacts while rewarding higher density and resolution.

To address these challenges, we propose a novel point quality evaluation metric (PQM) that provides a comprehensive and thorough assessment of point cloud quality. PQM comprises four sub-metrics, each evaluating a different aspect of point clouds’ quality:

- **Completeness:** Measures the proportion of missing data in a point cloud map. It is critical for applications such as autonomous driving and robotics, where having a complete point cloud is essential for ensuring safety.
- **Artifact Score:** Measures the proportion of non-existent artifacts added in error. It is useful in detecting the impact of artifacts on visual fidelity, especially in augmented reality and virtual environment creation.
- **Accuracy:** Measures how close the points are to their true positions. It is vital for infrastructure inspection and manufacturing quality control, where registration accuracy plays a crucial role.
- **Resolution:** Measures the density of the point cloud map. It is an indicator of how detailed the map is and can enhance fine-grained manipulation and object recognition precision.

In conclusion, PQM provides a comprehensive evaluation of point cloud quality by addressing various aspects of LiDAR maps, making it a valuable tool for several applications. The contributions of this paper are as follows:

- Propose PQM for evaluating point cloud maps.
- Provide an efficient multi-threaded implementation.

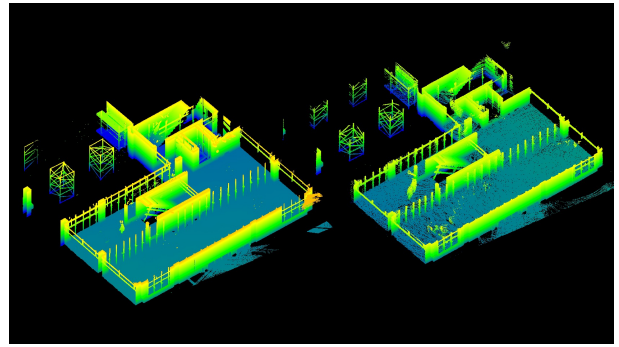


Fig. 2: Left: Ground truth from HILTI SLAM Dataset [4] using Z+F Imager 5016; Right: FAST-LIO2 using Hesai Pandar XT-32

- Evaluate the metric in simulation over three maps and 3 SLAM systems
- Perform an ablation study on the effect of mapping errors
- Provide an open-source suite to the research community to enable point cloud map quality evaluation. The GitHub link is in the abstract.

II. RELATED WORK

SLAM systems can produce point cloud maps with varying levels of density and fidelity using different sensors. Visual SLAM systems that use monocular cameras [5], stereo cameras [6], and RGBD cameras [7] to produce dense [7], [6] or sparse [5] point clouds have been proposed.

Recent advances in sensor technology, efficient libraries [8], [9], and faster computing have enabled real-time LiDAR mapping. Following [10] LiDAR SLAM systems have ever improved, both in localization and mapping performance.

There is a growing interest in dense 3D mapping using LiDAR SLAM. LOAM [10], LeGO-LOAM [2], LIO-SAM [11], LVI-SAM [12], LINS [13] and FAST-LIO2 [14], [1] generate relatively dense point clouds using online localization and mapping. Methods like Puma [3] and SHINE [15] output meshes by performing offline mapping and localization either solely with sequential LiDAR scans or with additional odometry information.

SLAM systems are generally evaluated for their localization and re-localization performance with the Absolute Trajectory Error (ATE) as seen in [16],[17],[18] with changes in environmental factors such as illumination. Although ATE is a good measure of a SLAM system’s localization performance, it is a poor measure of map quality. In some cases, ATE can be used to evaluate the overall structure of the map, not density and completeness. For example, ORB-SLAM [5] is known for good localization and tracking performance even though it produces sparse point cloud maps. In other cases, trajectory error may not be a sufficient metric to evaluate mapping performance. In [19], the authors use a WiFi-based distributed mapping system which cannot be evaluated with the ATE since a ground truth trajectory is hard to obtain in a distributed mapping scenario. Thus, the authors use known landmark (April tag [20]) positions to evaluate their system indicating a need for a metric to

evaluate the map quality directly.

Reconstruction error calculated over point clouds is a direct approach to evaluating map accuracy. Chamfer distance (CD), Hausdorff distance (HD), and Earth Mover’s distance (EMD) are popular distance metrics used in computing reconstruction error in point clouds [21],[3]. However, there are limitations in using distance-based reconstruction error as a performance metric to measure map quality.

For example, CD (Eq.1) is computed as the sum of distances in two point clouds, usually referred to as source and candidate. For each point in the source, the distance to its nearest neighbor in the candidate point cloud is computed and vice versa. The sum of distances over both point clouds is the CD. It is fast to compute and it can capture the overall similarity between two point clouds. However, it does not take into account the local variations and structural information in the point clouds, which can be important in some applications. Secondly, it is insensitive to density distribution. Finally, it is significantly influenced by outliers.

$$d_{Chamfer}(A, B) = \sum_{a \in A} \min_{b \in B} \|a - b\|_2 + \sum_{b \in B} \min_{a \in A} \|a - b\|_2 \quad (1)$$

As another example, HD (Eq. 2) is calculated as the maximum distance between two points in the source and candidate point clouds. This means that for each point in one point cloud, the distance to the farthest point in the other point cloud is calculated, and the maximum of all such distances is the HD. It captures the similarity between two point clouds, including their overall arrangement. However, it is computationally expensive to compute and is not as efficient as CD.

$$d_{Hausdorff}(A, B) = \max(\sup_{a \in A} d(a, B), \sup_{b \in B} d(A, b)) \quad (2)$$

Dense point clouds generated by some SLAM systems like FAST-LIO2 rival that of survey and engineering grade LiDARs as seen in (Fig. 2). This means they can be used for applications that need high-resolution point clouds such as GIS analysis [22], infrastructure inspection, 3D reconstruction, and object detection [23], [24] to name a few. With hardware and algorithmic advancements that produce such detailed point clouds, there is a need for a way to measure the difference in the quality of these point clouds. Popular metrics like CD, HD, and EMD have difficulty in capturing coverage, completeness, structural information, local variations in error, and are computationally expensive. Additionally, these methods do not account for artifacts or missing data and do not evaluate the components of quality discretely. Although methods like [25], [26], [27] exist, they focus on specific applications like visual quality and point cloud generation acting as a loss function for neural network training. [27] provides a way to measure the accuracy and completeness of meshes generated by multi-view stereo reconstruction but doesn’t account for resolution and artifacts [18] complains about the lack of ground truth to evaluate point clouds, we address this by using simulated datasets where ground truth from the simulation environment

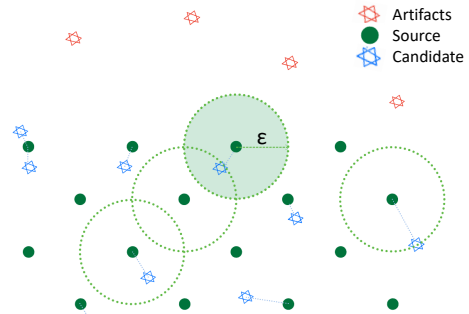


Fig. 3: Valid points - Candidate points within ϵ of source point are marked valid while others are marked invalid (artifacts)

is available in the form of meshes. We then sample these meshes to acquire ground truth point clouds.

Therefore, we propose the Point Quality Metric (PQM) which addresses some limitations of existing metrics, namely: (i) capturing a notion of map coverage, (ii) penalizing non-existent artifacts, (iii) measuring accuracy and, (iv) rewarding higher density and resolution. We believe our proposal provides a framework for the comprehensive evaluation of two point clouds based on their completeness, accuracy, artifacts, and resolutions.

III. METHOD

This section describes the proposed metric PQM and the evaluation framework including an ablation study to independently measure the effectiveness of each sub-metric. As mentioned above, point clouds generated by LiDAR SLAM methods although dense can be inaccurate and incomplete due to the path taken by the robot and registration errors. Further, these point clouds can contain artifacts (anomalies or points not present in ground truth) that degrade the overall quality.

A. Point Quality Metric (PQM)

We denote the source (ground truth) point cloud by $A = a_i$, which we refer to as pcd_A . Similarly, we denote the candidate point cloud by $B = b_i$, referred as pcd_B , where a_i and b_i are in R^d and $i = 1, \dots, N$. Our goal is to measure the difference in quality between the source point cloud pcd_A and the candidate point cloud pcd_B . Quality, as defined in Sec.III, is a weighted combination of the four sub-metrics: completeness, artifact score, accuracy, and resolution. Each sub-metric contributes to the overall quality of the point cloud, and evaluating them independently enables us to assess the effect of each sub-metric on the overall quality.

Q_{PQM} denotes the overall quality given by eq. 7 while Q_c , Q_t , Q_a and Q_r denote the individual sub-metrics completeness, artifact score, accuracy, and resolution respectively.

Region Splitting:

To efficiently evaluate large point clouds, we divide them into smaller regions of equal size or ”cells”, with each cell having a size of r . This enables to compare in parallel and provides insights into the quality of different areas within the point cloud. The point cloud is split into N such cells, and



Fig. 4: Simulation Worlds used for evaluation. Mai City (left), Village (center), Warehouse (right)

sub-metrics are computed for each cell. Cells are denoted as $cell_{A_j} \in pcd_A$ and $cell_{B_j} \in pcd_B$, where $j = 1 \dots N$. PQM is normalized between 0 and 1, where 1 represents the best quality and 0 represents the worst quality. In contrast, geometric distance metrics such as CD, HD, and EMD are typically calculated such that a score of 0 represents a perfect match, and any value greater than 0 represents a degree of mismatch.

1) *Resolution*: We define resolution per cell as the ratio of the density (pts/volume) of $cell_B$, a cell in pcd_B to density (pts/volume) of $cell_A$, a cell in pcd_A given in Eq.(3). Overall resolution (Q_r) is the mean of q_r over N cells. Resolution determines the level of detail in the point cloud. Low resolution can cause loss of texture and smaller objects making the point cloud unusable for applications that require high fidelity and detail.

$$q_r = \left(\frac{\rho_{cell_B}}{\rho_{cell_A}} \right) \quad (3)$$

2) *Accuracy*: Accuracy is measured as the ratio of the sum of distances between every point in $cell_B$, a cell in pcd_B to the nearest neighbor in $cell_A$, a cell in pcd_A given distance is less than threshold ϵ , to the product of the number of points in B and ϵ , given in (eq.4). The normalization is performed over $(|B| \times \epsilon)$ as this is the maximum distance possible if all points in $cell_B$ are valid (i.e. have neighbors within ϵ distance in $cell_A$). Overall accuracy (Q_a) is the mean of q_a over all N cells.

$$q_a = \left(1 - \left(\frac{1}{\epsilon |cell_B|} \right) \times \sum_{b \in cell_B} s(a, b) \right) \quad (4)$$

where,

$$s(a, b) = \begin{cases} \min_{a \in cell_A} \|a - b\|_2 & , \text{if } \min_{a \in cell_A} \|a - b\|_2 \leq \epsilon \\ 0 & , \text{otherwise} \end{cases}$$

3) *Completeness*: Completeness is the ratio of valid points (Fig. 3) of $cell_B$ (i.e. points within ϵ distance of $cell_A$) to the total points in $cell_A$ given by (eq.5). This gives us a measure of how complete a given region is compared to the ground truth and can be used to estimate missing areas in the candidate point cloud. Overall completeness is given by Q_c , the mean of all (q_c) over N cells.

$$q_c = \left(\frac{|\{b_i \in cell_B : \min_{a \in cell_A} \|a - b\|_2 \leq \epsilon\}|}{|cell_A|} \right) \quad (5)$$

4) *Artifact Score*: Artifacts (Fig. 3) are defined as the points in $cell_B$ but not in $cell_A$. These are generated due to reflections, distortion, or misregistration of points. Artifact

score is the ratio of valid points of $cell_B$ (i.e. points within ϵ distance of $cell_A$) to the total points in $cell_B$ given by (eq.6). Similar to III-A.3, the overall artifact score is given by (Q_t).

$$q_t = \left(\frac{|\{b_i \in cell_B : \min_{a \in cell_A} \|a - b\|_2 \leq \epsilon\}|}{|cell_B|} \right) \quad (6)$$

Overall Map Quality:

PQM is computed as the mean of the weighted sum of q_r, q_a, q_c , and q_t overall N cells. The weights $\{\omega_r, \omega_a, \omega_c, \omega_t\}$ correspond to each of these sub-metrics, respectively. For all experiments in this paper, we equally weight each sub-metric ($\{\omega_r, \omega_a, \omega_c, \omega_t\} = 0.25$) to ensure that they contribute equally to the overall quality score. However, these weights can be adjusted to meet the specific requirements of a given application.

$$Q_{PQM}(A, B, \epsilon) = \frac{1}{N} \sum_{j=1}^N (\omega_r \cdot q_r^j + \omega_a \cdot q_a^j + \omega_c \cdot q_c^j + \omega_t \cdot q_t^j) \quad (7)$$

B. Controlled Ablation Study

To evaluate PQM, we perform an ablation study using a prototype point cloud (Stanford Bunny [28]) model. The study involves applying various degradation to pcd_A , the source model, and using PQM, CD and HD to evaluate the quality at each step.

1) *Artifacts*: We add points to pcd_A to simulate artifacts (pcd_B is a copy of pcd_A with added artifacts), which can be caused by sensor noise or registration errors. A set percent(p) of points are added to each cell from a uniformly sampled sphere artifact $1/10^{th}$ the size of the cell, placed at the center of the cell. This also affects resolution since the number of points in pcd_B increases.

2) *Completeness*: A patch of points is removed from pcd_A to simulate incompleteness, which can be caused due to inconsistent mapping, down-sampling, and/or sensor noise. A set percent(p) of nearest neighbors of a randomly selected point are removed per cell.

3) *Accuracy*: Gaussian noise is added to pcd_A to simulate loss of accuracy. Gaussian noise is applied to the candidate point cloud with 0 μ and a finite σ value, where σ is the variance applied to the points in a random normal direction.

4) *Resolution*: Uniform down-sampling is applied to pcd_A to simulate the reduction in resolution and reduce the complexity of the point cloud while preserving its overall structure. This is achieved by sampling every k^{th} point in the current cell, where k is the control parameter.



Fig. 5: Ablation study. (a) Original unmodified point cloud (b) Arbitrary clusters added in error (c) Clusters of points removed to test completeness (d) Random points added with gaussian noise (50%) and (e) Points down-sampled to 20%

Fig. 5 shows the bunny model with 50% degradation (for artifacts, completeness, accuracy) and a sampling rate of 5 (for resolution) where pcd_A (green) is the source point cloud and pcd_B (red) are candidates after degradation.

C. Map Evaluation Framework

To further study PQM, we collect LiDAR scans in purpose-built simulation environments (Fig. 4) and build point cloud maps using several popular LiDAR SLAM systems. The simulation environments are built using the Gazebo simulator [29] and mesh models of the worlds. We simulate an Ouster OS1-128 LiDAR on a Clearpath Husky platform to collect the LiDAR scans. The simulation worlds include the outdoor world provided by the Mai-City dataset [3] and two other worlds called "Village" and "Warehouse" as seen in Fig. 4. The environments are designed to represent city blocks and warehouses, complete with buildings, trees, storage pallets, and other elements commonly found in the real world. The use of simulation allows for more controlled testing conditions, ground truth maps, and the generation of visual data from multiple views for testing and evaluation.

The candidate point clouds are generated using LeGO-LOAM [2], FAST-LIO2 [1], and Puma [3]. LeGO-LOAM stands for ground-optimized LiDAR odometry and mapping. The system outputs a dense point cloud and real-time odometry. FAST-LIO2 employs a tightly-coupled LiDAR+IMU method to generate dense point clouds in real time. This is achieved through the direct registration of scans with minimal downsampling facilitated by the use of an iKD-tree [30] for fast point-wise and block-wise operations. Puma [3] employs a unique approach to mesh generation by performing frame-to-mesh registration and Poisson Surface Reconstruction [31],[32] to generate a mesh. While this process is not real-time, the resulting meshes are lightweight and highly representative of the real world.

Finally, the point clouds generated by these methods (candidates) in the simulated worlds (Fig. 6) and their respective ground truths (source) are used to evaluate PQM. We also measure CD and HD between the candidate and source point clouds. The next section shows the comparative results.

IV. EXPERIMENTAL EVALUATION

PQM is implemented using Open3D [33] and PDAL [34] libraries and runs entirely on a desktop workstation with 6C/12T CPU and 32 GB of Memory. We also provide a CUDA accelerated implementation with PyTorch [35], which can be advantageous for large point clouds.

Experimental evaluation is performed on three simulation datasets, the HILTI dataset [4], and the Stanford bunny [28]. Candidate point clouds are evaluated against the source point cloud sampled from meshes which as mentioned earlier were used in the simulation worlds. Meshes are sampled into point clouds where the number of points is the maximum of all point clouds generated by the three SLAM methods.

A. Ablation Study

To evaluate the performance of PQM in isolation we degrade the source ([28]) point cloud as described in SEC. III-B. Experiments were performed for a range of degradation (0% to 90% with an increment of 5% and sampling rate of 1 to 19) with varying cell sizes i.e 0.05, 0.04, 0.03, 0.02 (meter). Fig. 7 shows results with cell size 0.05 (dividing the model into 4x4x3 cells). ϵ is maintained as half the average distance between points in pcd_A . ϵ is a tuneable parameter and can be chosen based on application. All trials are evaluated with weights $\{\omega_c, \omega_t, \omega_a, \omega_r\} = 0.25$, and $\epsilon = 0.0002$.

1) *Artifact Score:* Tab. I and Fig. 7 show adding artifacts proportionally decreases Q_t , while Q_a, Q_c are unchanged. Q_r also shows change due to the spherical artifact as mentioned in Sec.III-B.1

2) *Completeness:* Tab. I and Fig. 7 show completeness Q_c decreases as points are removed from pcd_A , while Q_a, Q_t are unchanged. Q_r also shows change due to the decrease in total points as mentioned in Sec.III-B.2

3) *Accuracy:* Tab. I and Fig. 7 show decrease in Q_a and in-turn in Q_{PQM} . σ for gaussian noise is constrained to $\epsilon = 0.0002$ to ensure Q_c and Q_t are not affected. The negligible change in other sub-metrics can be due to the overflow of boundary points. This demonstrates the efficacy of using PQM where deviations in accuracy might be small.

4) *Resolution:* Tab. I shows a decrease in resolution with an increase in sampling rate. This is unlike IV-A.2 as removing a continuous patch of points affects completeness more than resolution, while down-sampling degrades Q_r and Q_c almost equally, if not exactly as seen in Fig. 7.

5) *Chamfer and Hausdorff distance:* Similarly, Fig. 7, shows the change in CD and HD for each degradation. CD (green) shows a gradual increase, which signifies an increasing degradation in quality, but it fails to give insights about the type of quality that is affected. Further, its value is unbounded and hence cannot justify normalized quality value for a reasonable comparison. In the case of HD (blue), values do not show any correlation with the applied degradation.

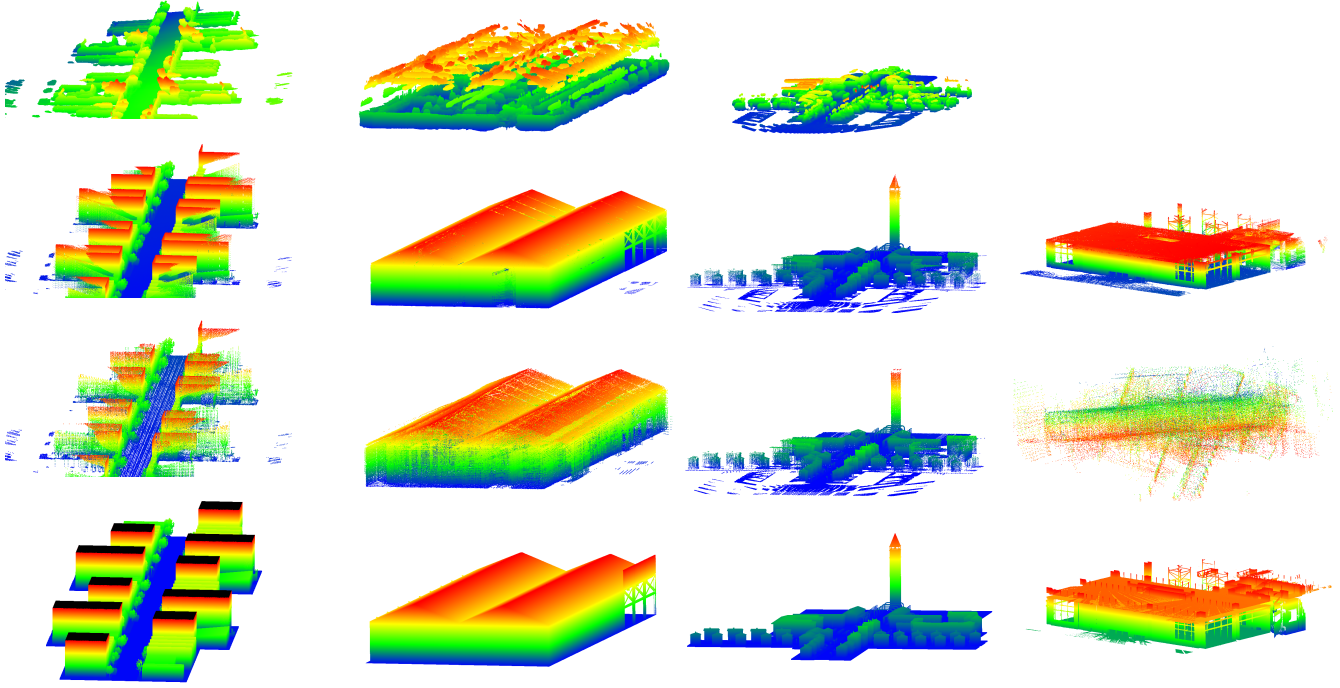


Fig. 6: Qualitative evaluation of SLAM systems. The figure shows, from top to bottom, dense maps generated using PUMA, FAST-LIO, LeGo-LOAM, and ground truth. Worlds from left to right are Mai-City, Warehouse, Village, and Exp04 sequence from the HILTI dataset

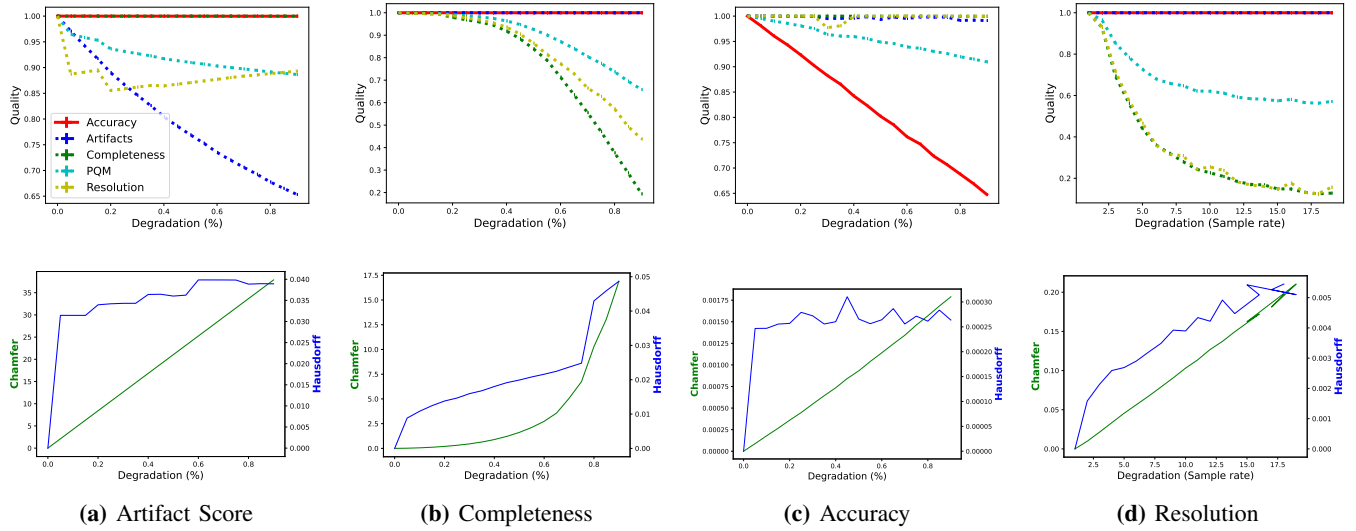


Fig. 7: Ablation Study. (a), (b), (c), and (d) depict the impact of adding artifacts, removing points, adding noise, and down-sampling on the proposed quality metrics, individual sub-metrics, CD and HD. Our method provides further insight into map quality.

TABLE I: Ablation Study

Target Sub-metric	Parameter	Candidate Pts	GT pts	$D_{chamfer}$	$D_{hausdorff}$	Q_r	Q_a	Q_c	Q_t	Q_{PQM}
Artifact Score (%)	25	213586	100106	10.5184	0.0342	0.8586	0.9999	1.0000	0.8676	0.9315
	50	256309	100106	21.0403	0.0360	0.8708	0.9999	1.0000	0.7692	0.9100
	75	299028	100106	31.5700	0.0398	0.8857	0.9998	1.0000	0.6926	0.8945
Completeness (%)	25	170877	100106	0.0004	0.0003	0.9998	0.9008	0.9999	0.9994	0.9749
	50	170877	100106	0.0009	0.0003	1.0000	0.8051	0.9999	0.9986	0.9509
	75	170877	100106	0.0015	0.0003	0.9999	0.7033	0.9996	0.9946	0.9244
Accuracy (%)	25	128168	100106	0.3108	0.0147	0.9768	1.0000	0.9688	1.0000	0.9864
	50	85445	100106	1.6109	0.0199	0.8645	1.0000	0.8395	1.0000	0.9260
	75	42726	100106	6.7446	0.0248	0.6278	1.0000	0.4713	1.0000	0.7748
Resolution (sample rate)	5	34187	100106	0.0455	0.0027	0.4666	1.0000	0.4399	1.0000	0.7266
	10	17099	100106	0.1031	0.0039	0.2553	1.0000	0.2266	1.0000	0.6205
	15	11406	100106	0.1624	0.0054	0.1481	1.0000	0.1491	1.0000	0.5743

TABLE II: Evaluation on SLAM Methods

Candidate	Method	Candidate Pts	GT pts	$D_{chamfer}$	$D_{hausdorff}$	Q_r	Q_a	Q_c	Q_t	Q_{PQM}
HILTI	LeGO LOAM	84761	6845275	1535250.251	6.4576	0.0023	0.4600	0.0010	0.0759	0.1348
	FAST-LIO2	5832076	6845275	602159.2716	5.5596	0.2177	0.3836	0.3681	0.4268	0.3491
Mai City	LeGO LOAM	268003	78513113	614644320.9	21.7358	0.0145	0.5940	0.0016	0.6559	0.3165
	FAST-LIO2	78513193	78513113	560122060.2	21.8017	0.3517	0.6244	0.2327	0.6994	0.4771
	Puma	78513052	78513113	1595554060	22.3074	0.2932	0.4689	0.0378	0.0736	0.2184
Village	LeGO LOAM	402346	53079602	235825489.3	54.1642	0.0593	0.6428	0.0005	0.1026	0.2013
	FAST-LIO2	53079702	53079602	256641433.7	53.8912	0.3061	0.7615	0.2214	0.4514	0.4351
	Puma	53079702	53079602	2595147655	35.0528	0.2858	0.3927	0.0667	0.0904	0.2089
Warehouse	LeGO LOAM	901658	111853794	31136219.94	13.7512	0.0051	0.7866	0.0015	0.2018	0.2487
	FAST-LIO2	111853794	111853794	475765579.7	12.9406	0.4961	0.7068	0.5190	0.8649	0.6467
	Puma	111853794	111853794	572566956.5	12.3049	0.4565	0.7498	0.2474	0.2937	0.4368

TABLE III: PQM with varying ϵ and r values (HILTI Exp04)

Method	r	ϵ	Q_r	Q_a	Q_c	Q_t	Q_{PQM}
FAST-LIO2	1	0.1	0.2054	0.3582	0.2435	0.3156	0.2807
LeGO-LOAM			0.0038	0.4139	0.0009	0.0519	0.1176
LeGO-LOAM	2		0.005	0.4727	0.001	0.0564	0.1338
FAST-LIO2			0.2059	0.3189	0.2651	0.3162	0.2765
LeGO-LOAM	5		0.0034	0.5077	0.0008	0.0447	0.1392
FAST-LIO2			0.1844	0.4241	0.2991	0.386	0.3234
LeGO-LOAM	1	0.01	0.0038	0.4385	0	0.0035	0.1115
FAST-LIO2			0.2054	0.5103	0.0097	0.0127	0.1845
LeGO-LOAM	2		0.005	0.4991	0.0001	0.0038	0.127
FAST-LIO2			0.2059	0.4725	0.0097	0.011	0.1748
FAST-LIO2	5		0.1844	0.6139	0.0111	0.0121	0.2054
LeGO-LOAM			0.0034	0.5284	0.0001	0.0033	0.1338

Results of these experiments show that PQM is effective in detecting and quantifying changes in map quality due to different types and levels of degradation. The scores generated by PQM correlate with the expected change in resulting value for each targeted sub-metric.

Overall, the experiment demonstrates the effectiveness of the PQM metric in evaluating the quality of point clouds and detecting changes in map quality due to different types and levels of degradation and hence can act as a tool to detect point cloud suitability for specific applications.

B. Evaluation on SLAM systems

The performance of PQM on large, realistic point cloud maps generated using the SLAM systems mentioned above was evaluated exhaustively in three simulated worlds and the exp04 sequence of the HILTI dataset. The results of this evaluation are presented in Fig. 6, which shows the qualitative differences between the maps generated by the SLAM systems and the ground truth. Tab. II shows the sub-metrics for each map. Each sub-metric evaluates a certain aspect of quality as defined in Sec. III. PQM is computed as the weighted sum of these sub-metrics, where the weights (Eq. 7) are set by users based on application. For all evaluations, the weights were set to 0.25, making the contribution of each sub-metric equal for overall quality. We also set $\epsilon = 0.1$ and cell size $r = 10$ for all tests in Tab. II. More suitable values were not explored for all maps due to long computing times. A study of the effect of ϵ and r is shown in Tab. III.

Visually, it is apparent that the FAST-LIO2 generates the highest-quality maps compared to other methods in terms

of resolution, completeness, and accuracy. However, the highlighted CD and HD distance values in Tab. II do not reflect this observation. We can see that CD and HD distances only correctly identify the best map 1/4 and 0/4 times, respectively. On the other hand, PQM consistently identifies point clouds generated by FAST-LIO2 as the ones with the highest overall quality. The sub-metrics are also indicative of PQM's performance, with only Q_a being incorrect in 2 instances (HILTI and Warehouse). This is likely due to the threshold of $\epsilon = 0.1$ used. However, a lower ϵ value correctly identifies Q_a , as seen in Tab. III. Highlighted values show that as ϵ is reduced ($\epsilon = 0.01$), quality is calculated correctly 2/3 times, which is much greater.

V. DISCUSSION

Need for reference point clouds: For the scope of this paper, we assume that candidate maps are compared against ground truth point clouds or meshes. While acquiring the ground truth maps can be difficult in real-world scenarios, we make the following observations: (i) To effectively quantify the mapping performance of a SLAM system a ground truth or reference is necessary, (ii) Ground truth can be generated using an engineering grade LiDAR which can generate centimeter-accurate if not millimeter-accurate point clouds ([4], Fig. 2), and (iii) Alternatively, we can evaluate in simulation where ground truth is readily available. Recent advancements in high fidelity simulators [36], [37] make this a lucrative option. Our evaluation framework uses three simulation scenarios as shown in Figure 4.

Customizability: While we provide one holistic PQM metric, the intent is to expose the various dimensions of importance as highlighted by the submetrics - completeness, artifact score, accuracy and resolution. We envision the user customizing the weights and the various parameters to better suit their application. This will allow better quantification of map quality. On those lines, the introduction of cell size r and threshold ϵ enables the user to tune PQM to a particular use case. The smaller the ϵ the lower the tolerance is for accuracy, completeness, and artifact score. The cell size helps reduce the computational complexity for large point clouds, metrics can be computed in parallel, and as cell size is decreased the resolution for local variations increases.

VI. CONCLUSION

We propose a novel point quality evaluation metric (PQM) that comprehensively evaluates the quality of dense point cloud maps generated by SLAM algorithms. PQM is designed to capture aspects of mapping accuracy that are not addressed by existing evaluation metrics and can help improve the performance of SLAM algorithms in various applications. The experimental results presented in this paper demonstrate the effectiveness and robustness of PQM in evaluating the quality of point clouds. We open-source our evaluation framework with extensive documentation for others to use the PQM metric in their evaluation of dense mapping methods.

REFERENCES

- [1] W. Xu, Y. Cai, D. He, J. Lin, and F. Zhang, "FAST-LIO2: Fast Direct LiDAR-Inertial Odometry," *IEEE Transactions on Robotics*, pp. 1–21, 2022. Conference Name: IEEE Transactions on Robotics.
- [2] T. Shan and B. Englot, "LeGO-LOAM: Lightweight and Ground-Optimized Lidar Odometry and Mapping on Variable Terrain," in *2018 IEEE/RSJ International Conference on Intelligent Robots and Systems (IROS)*, (Madrid), pp. 4758–4765, IEEE, Oct. 2018.
- [3] I. Vizzo, X. Chen, N. Chebroly, J. Behley, and C. Stachniss, "Poisson Surface Reconstruction for LiDAR Odometry and Mapping," in *2021 IEEE International Conference on Robotics and Automation (ICRA)*, (Xi'an, China), pp. 5624–5630, IEEE, May 2021.
- [4] L. Zhang, M. Helmerger, L. F. T. Fu, D. Wisth, M. Camurri, D. Scaramuzza, and M. Fallon, "Hilti-Oxford Dataset: A Millimetre-Accurate Benchmark for Simultaneous Localization and Mapping," 2022. Publisher: arXiv Version Number: 1.
- [5] R. Mur-Artal and J. D. Tardós, "Orb-slam2: An open-source slam system for monocular, stereo, and rgb-d cameras," *IEEE Transactions on Robotics*, vol. 33, pp. 1255–1262, Oct 2017.
- [6] M. Labbé and F. Michaud, "Online global loop closure detection for large-scale multi-session graph-based slam," in *2014 IEEE/RSJ International Conference on Intelligent Robots and Systems*, pp. 2661–2666, Sept 2014.
- [7] F. Endres, J. Hess, J. Sturm, D. Cremers, and W. Burgard, "3-d mapping with an rgb-d camera," *IEEE Transactions on Robotics*, vol. 30, pp. 177–187, Feb 2014.
- [8] S. Agarwal, K. Mierle, and T. C. S. Team, "Ceres Solver," 3 2022.
- [9] R. B. Rusu and S. Cousins, "3D is here: Point Cloud Library (PCL)," in *IEEE International Conference on Robotics and Automation (ICRA)*, (Shanghai, China), May 9-13 2011.
- [10] J. Zhang and S. Singh, "LOAM: Lidar Odometry and Mapping in Real-time," in *Robotics: Science and Systems X*, Robotics: Science and Systems Foundation, July 2014.
- [11] T. Shan, B. Englot, D. Meyers, W. Wang, C. Ratti, and D. Rus, "LIO-SAM: Tightly-coupled Lidar Inertial Odometry via Smoothing and Mapping," 2020. Publisher: arXiv Version Number: 3.
- [12] T. Shan, B. Englot, C. Ratti, and D. Rus, "LVI-SAM: Tightly-coupled Lidar-Visual-Inertial Odometry via Smoothing and Mapping," in *2021 IEEE International Conference on Robotics and Automation (ICRA)*, pp. 5692–5698, May 2021. ISSN: 2577-087X.
- [13] C. Qin, H. Ye, C. E. Pranata, J. Han, S. Zhang, and M. Liu, "LINS: A Lidar-Inertial State Estimator for Robust and Efficient Navigation," in *2020 IEEE International Conference on Robotics and Automation (ICRA)*, (Paris, France), pp. 8899–8906, IEEE, May 2020.
- [14] W. Xu and F. Zhang, "FAST-LIO: A Fast, Robust LiDAR-Inertial Odometry Package by Tightly-Coupled Iterated Kalman Filter," *IEEE Robotics and Automation Letters*, vol. 6, pp. 3317–3324, Apr. 2021.
- [15] X. Zhong, Y. Pan, J. Behley, and C. Stachniss, "Shine-mapping: Large-scale 3d mapping using sparse hierarchical implicit neural representations," in *Proceedings of the IEEE International Conference on Robotics and Automation (ICRA)*, 2023.
- [16] M. Bujanca, X. Shi, M. Spear, P. Zhao, B. Lennox, and M. Lujan, "Robust SLAM Systems: Are We There Yet?," Sept. 2021. arXiv:2109.13160 [cs].
- [17] J. Sturm, N. Engelhard, F. Endres, W. Burgard, and D. Cremers, "A benchmark for the evaluation of rgb-d slam systems," in *2012 IEEE/RSJ International Conference on Intelligent Robots and Systems*, pp. 573–580, 2012.
- [18] F. Endres, J. Hess, N. Engelhard, J. Sturm, D. Cremers, and W. Burgard, "An evaluation of the rgb-d slam system," in *2012 IEEE International Conference on Robotics and Automation*, pp. 1691–1696, 2012.
- [19] C. Adhivarahan and K. Dantu, "Wisdom: Wireless sensing-assisted distributed online mapping," in *2019 International Conference on Robotics and Automation (ICRA)*, p. 8026–8033, IEEE Press, 2019.
- [20] J. Wang and E. Olson, "AprilTag 2: Efficient and robust fiducial detection," in *Proceedings of the IEEE/RSJ International Conference on Intelligent Robots and Systems (IROS)*, October 2016.
- [21] H. Fan, H. Su, and L. Guibas, "A Point Set Generation Network for 3D Object Reconstruction from a Single Image," in *2017 IEEE Conference on Computer Vision and Pattern Recognition (CVPR)*, pp. 2463–2471, July 2017. ISSN: 1063-6919.
- [22] Y. Xie, J. Tian, and X. X. Zhu, "A review of point cloud semantic segmentation," *CoRR*, vol. abs/1908.08854, 2019.
- [23] C. Xu, B. Wu, Z. Wang, W. Zhan, P. Vajda, K. Keutzer, and M. Tomizuka, "SqueezeSegV3: Spatially-Adaptive Convolution for Efficient Point-Cloud Segmentation," in *Computer Vision – ECCV 2020* (A. Vedaldi, H. Bischof, T. Brox, and J.-M. Frahm, eds.), vol. 12373, pp. 1–19, Cham: Springer International Publishing, 2020.
- [24] Y. Zhou and O. Tuzel, "VoxelNet: End-to-End Learning for Point Cloud Based 3D Object Detection," Nov. 2017. arXiv:1711.06396 [cs].
- [25] A. Javaheri, C. Brites, F. Pereira, and J. Ascenso, "Joint geometry and color projection-based point cloud quality metric," *IEEE Access*, vol. 10, pp. 90481–90497, 2022.
- [26] J. Z. T. W. Z. L. D. L. Tong Wu, Liang Pan, "Density-aware chamfer distance as a comprehensive metric for point cloud completion," in *In Advances in Neural Information Processing Systems (NeurIPS)*, 2021, 2021.
- [27] S. Seitz, B. Curless, J. Diebel, D. Scharstein, and R. Szeliski, "A comparison and evaluation of multi-view stereo reconstruction algorithms," in *2006 IEEE Computer Society Conference on Computer Vision and Pattern Recognition (CVPR'06)*, vol. 1, pp. 519–528, 2006.
- [28] "Stanford bunny dataset, <https://graphics.stanford.edu/data/3dscanrep/>."
- [29] N. Koenig and A. Howard, "Design and use paradigms for gazebo, an open-source multi-robot simulator," in *2004 IEEE/RSJ International Conference on Intelligent Robots and Systems (IROS)* (IEEE Cat. No.04CH37566), vol. 3, pp. 2149–2154 vol.3, 2004.
- [30] Y. Cai, W. Xu, and F. Zhang, "ikd-Tree: An Incremental K-D Tree for Robotic Applications," Feb. 2021. arXiv:2102.10808 [cs].
- [31] M. Kazhdan, M. Bolitho, and H. Hoppe, "Poisson Surface Reconstruction," in *Symposium on Geometry Processing* (A. Sheffer and K. Polthier, eds.), The Eurographics Association, 2006.
- [32] M. Kazhdan and H. Hoppe, "Screened poisson surface reconstruction," *ACM Transactions on Graphics*, vol. 32, pp. 1–13, June 2013.
- [33] Q.-Y. Zhou, J. Park, and V. Koltun, "Open3D: A modern library for 3D data processing," *arXiv:1801.09847*, 2018.
- [34] P. Contributors, "PDAL Point Data Abstraction Library," Aug. 2020. Language: en.
- [35] A. Paszke, S. Gross, F. Massa, A. Lerer, J. Bradbury, G. Chanan, T. Killeen, Z. Lin, N. Gimelshein, L. Antiga, A. Desmaison, A. Kopf, E. Yang, Z. DeVito, M. Raison, A. Tejani, S. Chilamkurthy, B. Steiner, L. Fang, J. Bai, and S. Chintala, "Pytorch: An imperative style, high-performance deep learning library," in *Advances in Neural Information Processing Systems 32* (H. Wallach, H. Larochelle, A. Beygelzimer, F. d'Alché-Buc, E. Fox, and R. Garnett, eds.), pp. 8024–8035, Curran Associates, Inc., 2019.
- [36] S. Shah, D. Dey, C. Lovett, and A. Kapoor, "Airsim: High-fidelity visual and physical simulation for autonomous vehicles," in *Field and Service Robotics*, 2017.
- [37] F. Xia, A. R. Zamir, Z.-Y. He, A. Sax, J. Malik, and S. Savarese, "Gibson Env: real-world perception for embodied agents," in *Computer Vision and Pattern Recognition (CVPR)*, 2018 IEEE Conference on, IEEE, 2018.